Ozone-forced Southern Annular Mode during Antarctic Stratospheric Warming Events

Martin Jucker[1] and Rishav Goyal[1]

[1]University of New South Wales

November 30, 2022

Abstract

In 2019 southern hemisphere spring, a strong stratospheric warming event was predicted to force the southern annular mode (SAM) into a negative phase and adversely impact surface weather and Australian bushfire season for several months. Even though the negative SAM materialized towards late spring and summer, it was delayed by more than a month compared to model forecasts. Instead, the immediate surface response was a positive SAM through September and much of October. Here we show that the immediate surface response was a result of circulation changes forced by anomalously high ozone concentrations which occur during stratospheric warming events. The longer term tropospheric response was well predicted and is due to a different process acting on longer time scales. Capturing this coupling between dynamics and radiation in models is only possible with the inclusion of interactive ozone, which explains why most seasonal forecasting systems failed to capture it.

Ozone-forced Southern Annular Mode during Antarctic Stratospheric Warming Events

M. Jucker[1], **R. Goyal**[1]

[1]Climate Change Research Centre, University of New South Wales, Sydney, Australia

Key Points:

- Antarctic weak vortex events feature anomalous stratospheric heating via ozone increase.
- This heating forces a positive southern annular mode in the troposphere via dynamical feedbacks.
- The dynamical feedbacks are tied to increased stratospheric static stability.

Corresponding author: Martin Jucker, `publications@martinjucker.com`

Abstract

In 2019 southern hemisphere spring, a strong stratospheric warming event was predicted to force the southern annular mode (SAM) into a negative phase and adversely impact surface weather and Australian bushfire season for several months. Even though the negative SAM materialized towards late spring and summer, it was delayed by more than a month compared to model forecasts. Instead, the immediate surface response was a positive SAM through September and much of October. Here we show that the immediate surface response was a result of circulation changes forced by anomalously high ozone concentrations which occur during stratospheric warming events. The longer term tropospheric response was well predicted and is due to a different process acting on longer time scales. Capturing this coupling between dynamics and radiation in models is only possible with the inclusion of interactive ozone, which explains why most seasonal forecasting systems failed to capture it.

Plain Language Summary

In September of 2019, a rare event in the upper atmosphere was predicted to influence surface weather and worsen Australian bushfire season for several months. Even though that surface impact eventually appeared, it was delayed by more than a month compared to forecasts. Instead, the immediate surface response was opposite to what was expected through September and much of October. Here we show that the immediate surface response was a result of the unusually high ozone concentrations which occur during such stratospheric events with a very small ozone hole. Current forecasting systems do not include the role of stratospheric ozone, which explains why they were unable to predict the worsening of the drought and severe fire weather in 2019 spring.

1 Introduction

The spring 2019 stratospheric warming event (SWE, Methods) in the Southern Hemisphere (SH) was accompanied by a vertical dipole in polar cap (60-90°S) geopotential height throughout September and much of October, with positive anomalies in the stratosphere and negative anomalies in the troposphere (Fig. 1a)). As the event evolved in time, the stratospheric positive anomalies started to descend, and by late October the tropospheric anomalies switched signs to become positive as well. Positive polar cap geopotential height anomalies correspond to the negative phase of the Northern and Southern Annular Modes (NAM/SAM, Methods) (Gerber et al., 2010) and have long been associated with SWEs (Baldwin & Dunkerton, 2001). SWEs have attracted interest for their potential to improve seasonal forecasting in both hemispheres (Sigmond et al., 2013; Domeisen et al., 2020; Lim et al., 2019). Specifically, the negative phase of the SAM is associated with warmer and drier than usual conditions over much of Australia and South Africa, and the inverse for southern South America and New Zealand (Gillett et al., 2006).

However, the observation of a prominent and persistent positive phase of the tropospheric SAM during the SWE of 2019 was surprising (Fig. 1b)), and most forecasting systems predicted a much faster transition from neutral to negative SAM during 2019 spring (Rao et al., 2020). While the classic El Niño Southern Oscillation indices were neutral during 2019, there was a Central Pacific El Niño, which has been linked to the negative SAM during late spring and summer (Lim et al., 2021). There was also a strong positive Indian Ocean Dipole (IOD) during the spring of 2019, but the correlation between IOD and SAM in Austral spring is smaller than 0.1 (Supplementary), meaning that while the IOD may be important for South Eastern Australia rainfall (Ummenhofer et al., 2009), it is not a major driver of the (global) SAM during the season of interest here.

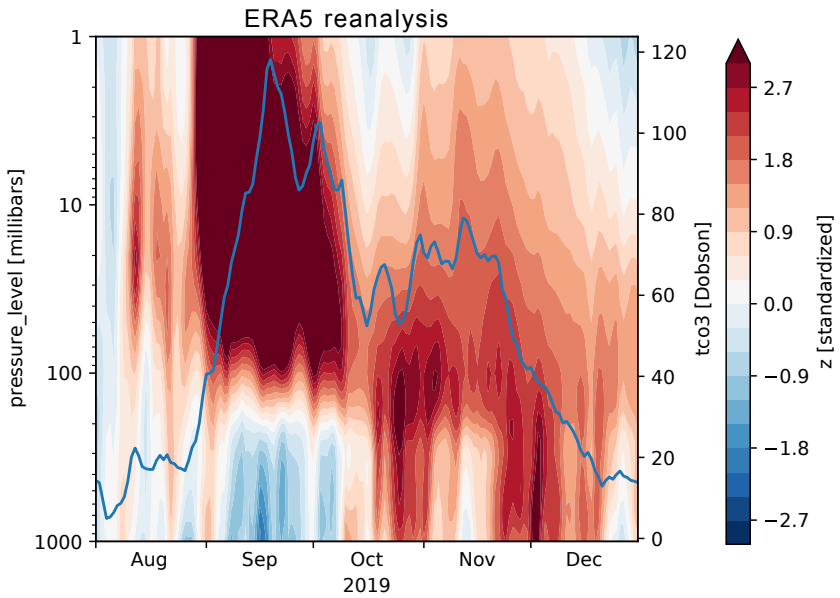

(a) Standardized polar cap geopotential height anomalies (shading) and total column ozone anomalies (line). Due to the relation between geopotential height and the southern annular mode, blue shading corresponds to positive SAM and red shading to negative SAM.

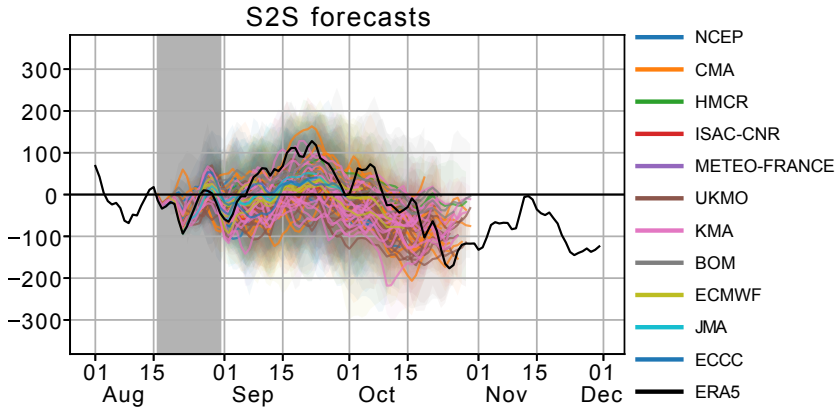

(b) S2S model forecasts from second half of August 2019. Shown is anomaly of 30-60S minus 60-90S geopotential height. Here positive values correspond to positive SAM. Each line corresponds to one ensemble mean forecast from one model. Shading denotes the forecast range across members for each forecast and model.

Figure 1. Spring 2019 anomalies in (a) ERA5 and (b) S2S seasonal forecasts. In (a), the vertical dipole during September and the first half of October, and the close relation between the geopotential height and ozone anomalies are clearly visible. In (b), most forecasts produce the negative SAM in response to the SSW, but fail to include the extended period of positive SAM in September and early October.

2 The role of stratospheric ozone

There is a close relationship between ozone and geopotential height anomalies in the stratosphere (compare shading and line in Fig. 1a)). This can be explained by the dynamically forced stratospheric circulation and the associated increase in poleward stratospheric ozone transport and diabatic heating due to downwelling at higher latitudes (Randel & Cobb, 1994). A warmer and weaker stratospheric polar vortex naturally exhibits higher geopotential heights, and limits ozone-reducing chemical reactions, which together with the increased meridional transport of ozone rich air from the tropics are responsible for the anomalously high stratospheric ozone concentrations (Plumb, 2002; Safieddine et al., 2020). The impact on the troposphere, however, is not trivial, and we will now show that the radiative impact of lower stratospheric ozone anomalies can explain the simultaneous negative tropospheric geopotential height anomalies.

Studies of tropospheric effects of stratospheric ozone anomalies have been conducted in the context of the forming and recovery of the ozone hole, and have consistently found that a positive tropospheric SAM is associated with a decrease in stratospheric ozone (Arblaster & Meehl, 2006; D. W. J. Thompson et al., 2011; Arblaster et al., 2011; McLandress et al., 2011) (i.e. the forming of the ozone hole), which for the case of a SWE (i.e. increased ozone) translates into a negative SAM and is again consistent with earlier work (D. W. J. Thompson et al., 2005; Lim et al., 2019). However, most of these studies focus on surface impacts in summer (December-February, DJF), and not in spring, which–at least in 2019–showed the inverse behavior of a positive SAM in the troposphere associated with a SWE. While there is sparse evidence of inverse surface impact of ozone depletion during Austral spring compared to summer (Hurrel & Van Loon, 1994), this hasn't attracted much attention until now and the dynamical processes responsible for this behavior are largely unknown.

3 Process studies

We designed custom numerical experiments to test how the full 3D ozone anomalies during the 2019 SWE may affect the tropospheric circulation (Methods), as lower stratospheric heating has been shown to have an influence on tropospheric dynamics (Simpson et al., 2009). Briefly, we conducted two experiments to make the results more robust, one with a full atmospheric General Circulation Model (Community Atmosphere Model, CAM4, Neale et al. (2010)) and one with an idealized moist model (Model of an idealized Moist Atmosphere, MiMA, Jucker and Gerber (2017)), both with fixed sea surface temperatures (SSTs). We then analysed the differences between simulations with 2005-2015 climatological ozone and a hybrid ozone concentration with 2019 spring ozone but climatological ozone during the other seasons (Methods). A major difference between the model simulations and 2019 observations is that the models are not forced into producing an actual SWE, as radiative forcing from anomalous ozone is the only forcing in our experiments and without additional dynamical forcing this is too weak to produce a 2019-like warming. Two important distinctions between the two model setups is that while CAM4 is a comprehensive atmospheric model, MiMA is used here without seasonal cycle, and it does not include clouds. The comparisons between CAM4 and MiMA therefore allow for additional assessments of the relative importance of cloud feedbacks (Grise et al., 2013) and seasonal cycle. In addition, having fixed surface temperatures in both models precludes any influence of longwave radiative effects on surface temperatures (Grise et al., 2009).

Despite their differences, both CAM4 and MiMA produce the vertical dipole in polar cap geopotential height anomalies during spring, which gradually changes into the familiar positive anomalies throughout the vertical column at longer time scales (Figs. 2a), 2b)). In latitude-pressure space, these springtime geopotential height anomalies correspond to the negative phase of the SAM in the stratosphere and the

positive phase in the troposphere (Gerber & Vallis, 2009) in both models and reanalysis (Fig. 2c), shading). In the troposphere, there is a clockwise anomalous circulation (solid contours) centred around 50-70°S, which explains the negative geopotential height anomalies at high latitudes and positive anomalies in midlatitudes. At the same time, the models show anomalously weak upward and stronger than usual equatorward Eliassen-Palm (EP) flux propagation in the upper troposphere around the same latitudes (arrows). We note that in reanalysis, the SWE is forced by stronger than usual upward EP fluxes, but in high latitudes in the troposphere a similar picture emerges as in the model simulations without SWE (Fig. 2c), right).

The equatorward deflection of otherwise upward propagating EP fluxes causes an anomalous divergence in the upper troposphere/lower stratosphere (Fig. 2d), solid contours). This in turn forces a local clockwise circulation via downward control (Methods). The reason why EP fluxes are deflected equatorward instead of propagating into the high latitude stratosphere is an increase in lower stratospheric stability due to anomalous ozone heating (Fig. 2d), shading).

At the same time, a slower response occurs which resembles the 'canonical' evolution of SWEs (Baldwin & Dunkerton, 2001; Charlton & Polvani, 2007; Jucker, 2016) (Fig. 3): After an initial fast dynamical response to stratospheric heating which takes place mostly in the troposphere as described above, the weakened polar vortex and decreased stability in the upper stratosphere locally favors anomalous upward EP flux, negative divergence and therefore a clockwise circulation with downwelling at high latitudes in the upper stratosphere (left panels in Figs. 3a),3b)). This causes the stratospheric perturbation to propagate downwards and by early summer the troposphere also switches to a negative SAM (right panels in Figs. 3a),3b)). We note that in the perpetual September simulation (top row if Fig. 3) the downward propagation is less pronounced, indicating that the seasonal cycle also plays a role at this stage, but the switch from positive to negative tropospheric SAM still occurs due to an inversion of EP flux divergence around the midlatitude tropopause (Fig. 3b), top right).

To check the sensitivity to the seasonal cycle, we ran two additional experiments with MiMA where the solar forcing corresponds to 30 days earlier in the year (i.e. August) and 30 days later (i.e. October). Surface temperatures, ozone concentrations and initial conditions remained unchanged. We find that the same ozone perturbation in late winter does not produce a consistent positive tropospheric SAM (Fig. S2(a)), which we attribute to the missing ozone heating when incoming sunlight is much weaker. Later in spring the stratospheric negative SAM propagates downward into the troposphere more quickly due to the weaker polar vortex base state (Fig. S2(b)).

4 Increased lower stratospheric stability leads to positive tropospheric SAM

The emerging picture of the mechanisms can be summarized as follows (Fig. 4): As a SWE is triggered, stratospheric ozone is transported from low to high latitudes. At the same time, the stratospheric polar vortex is both warmer and less isolated, inhibiting the formation of the ozone hole (Safieddine et al., 2020). Ozone concentrations increase most in the lower stratosphere and–if the event happens in the spring when enough sunlight is available–result in localized anomalous heating close to the tropopause. The heating of the lower stratosphere in turn increases the troposphere-stratosphere contrast in static stability, causing perturbations from the troposphere to travel horizontally within the upper troposphere rather than vertically into the stratosphere (Chen & Robinson, 1992). The deflection of EP fluxes creates anomalous divergence, which in turn forces a localised clockwise tropospheric circulation via downward control. That circulation includes anomalous upwelling over the polar cap and downwelling at lower latitudes, which strongly projects onto the positive phase

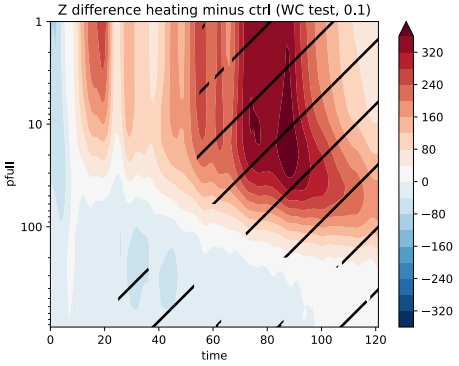

(a) September-December evolution of polar cap geopotential height anomalies in CAM4.

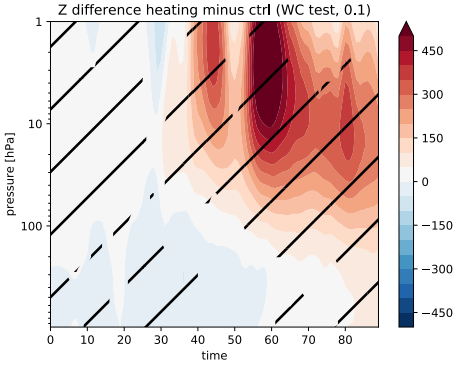

(b) 90-day evolution of polar cap geopotential height anomalies in perpetual September simulations in MiMA.

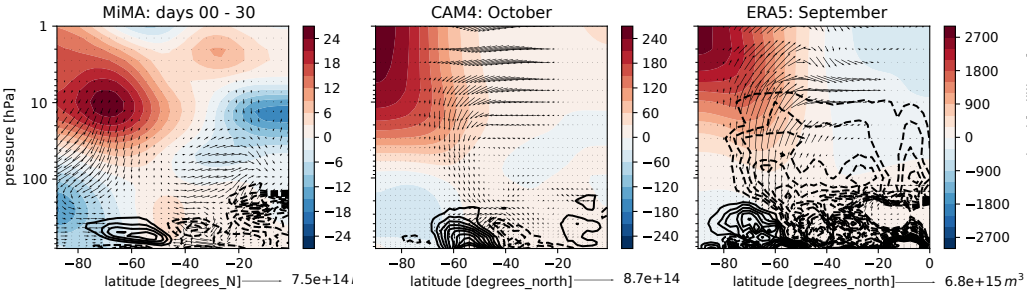

(c) Geopotential height (shading), streamfunction (contours) and EP flux anomalies (arrows).

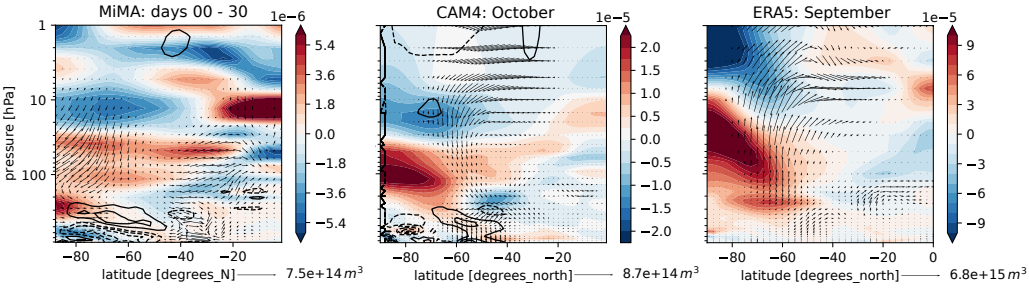

(d) Static stability (shading), EP flux divergence (contours) and EP flux anomalies (arrows).

Figure 2. Response to 2019 ozone heating compared to 2005-2015 climatology (Methods).In (c,d) the left panel shows results from MiMA perpetual simulations, the middle panel CAM4 mean October, and the right panel mean September anomalies. For both models we focus on time periods where the tropospheric response in (a,b) is negative and significant. Geopotential height is shown in meters, streamfunction in multiples of 1e9 kg/s, EP flux divergence in multiples of 0.5 $\mathrm{ms}^{-1}\mathrm{d}^{-1}$. EP flux arrow scale (Jucker, 2021b) is shown in each panel.

.

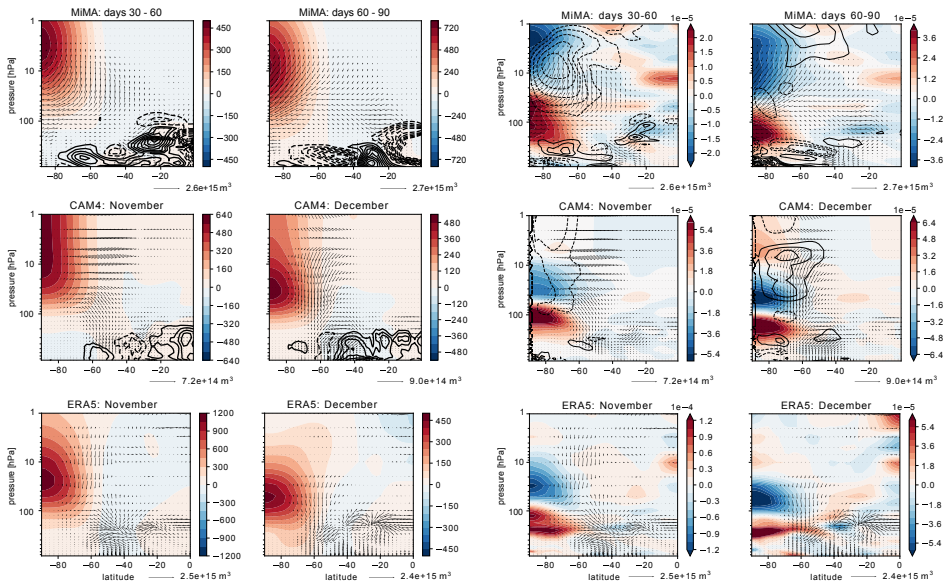

(a) As in Fig. 2(c) but for later lags.

(b) As in Fig. 2(d) but for later lags.

Figure 3. Longer term evolution for both models and reanalysis. All show qualitatively similar behaviour, with CAM4 remarkably close to reanalysis. Streamfunction and EP flux divergence was removed from ERA5 panels (bottom) due to low signal to noise ratio.

of the Southern Annular Mode. This anomalous circulation is synchronous with the amplitude of stratospheric ozone anomalies and the stratospheric warming. We note that similar vertical dipoles co-occurring with peaks of polar stratospheric ozone can be observed in other years in reanalysis (Supplementary, Fig. S1). Also, an early study focusing on the effects of ozone depletion (i.e. inverse sign from this study) briefly reports a sea surface pressure anomaly similar to the negative SAM during September-October (Hurrel & Van Loon, 1994).

On slightly longer time scales, the continuous stratospheric heating due to increased ozone concentrations (and during a SWE dynamical heating) both weakens the polar vortex and decreases static stability in the upper stratosphere. With time, this allows more EP fluxes to propagate into the upper stratosphere and cause locally increased convergence, forcing a clockwise circulation in the stratosphere. This signal then propagates downward similar to SWEs (Plumb & Semeniuk, 2003), and eventually forces an anomalous clockwise circulation in the troposphere as well, resulting in a negative tropospheric SAM in summer. We note that while the real evolution in 2019 includes the full effect of the sudden stratospheric warming, our model simulations only include the anomalous ozone heating. Even so, our model simulations are able to reproduce the initially positive tropospheric SAM and the switch to negative SAM by early summer, albeit somewhat weaker and slower.

While many seasonal forecasting systems still use zonally averaged ozone concentrations, previous work reported improvements in model simulations when using fully three-dimensional ozone rather than zonally averaged ozone (Rae et al., 2019). We have extended our analysis to model runs with zonal mean ozone (but otherwise identical to the simulations reported here), and found that the impact of perturbed ozone was weaker, but qualitatively similar (not shown). We conclude that while zonally asymmetric ozone seems to be important to reproduce circulation anomalies of

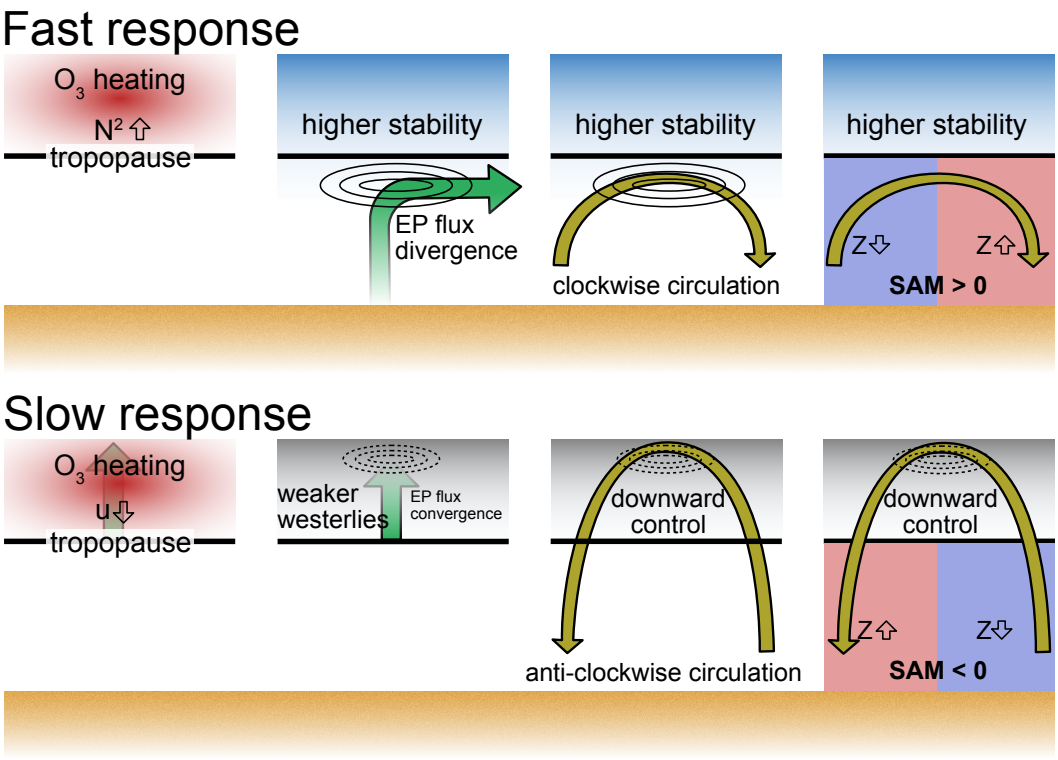

Figure 4. Schematic of the physical processes. The thick black line denotes the tropopause in all panels. The fast response (top) forced the positive SAM in September/October 2019, whereas the slow response (bottom) corresponds to the more conventional 'downward propagation' of the stratospheric signal which then influences the SAM on the longer timescale (negative phase). See text for more details.

similar amplitude, including dynamically driven perturbations (even if zonally averaged) seems to be the more important development step (Hendon et al., 2020). But in contrast to earlier studies, we find that including ozone perturbations in forecasting systems would improve model performance not only during Austral summer (Rae et al., 2019; Hendon et al., 2020) but also during spring.

Acknowledgements

Both authors acknowledge support by the ARC Centre of Excellence for Climate Extremes which is supported by the Australian Research Council via grant CE170100023. MJ further acknowledges ARC grant FL150100035. This research was undertaken with the assistance of resources from the National Computational Infrastructure (NCI Australia), an NCRIS enabled capability supported by the Australian Government. Model data is available at `doi.org/10.5281/zenodo.5120972`.

References

Andrews, D. G., Holton, J. R., & Leovy, C. B. (1987). *Middle Atmosphere Dynamics*. San Diego: Academic Press.

Andrews, D. G., Mahlman, J. D., & Sinclair, R. W. (1983, 12). Eliassen-Palm Diagnostics of Wave-Mean Flow Interaction in the GFDL "SKYHI" General Circulation Model. *Journal of the Atmospheric Sciences*, *40*(12),

2768–2784. Retrieved from http://journals.ametsoc.org/doi/abs/10.1175/1520-0469%281983%29040%3C2768%3AETWATM%3E2.0.CO%3B2 doi: 10.1175/1520-0469(1983)040⟨2768:ETWATM⟩2.0.CO;2

Andrews, D. G., & McIntyre, M. E. (1976, 11). Planetary Waves in Horizontal and Vertical Shear: The Generalized Eliassen-Palm Relation and the Mean Zonal Acceleration. *Journal of the Atmospheric Sciences*, *33*(11), 2031–2048. Retrieved from http://journals.ametsoc.org/doi/abs/10.1175/1520-0469%281976%29033%3C2031%3APWIHAV%3E2.0.CO%3B2 doi: 10.1175/1520-0469(1976)033⟨2031:PWIHAV⟩2.0.CO;2

Andrews, D. G., & McIntyre, M. E. (1978). Generalized Eliassen-Palm and Charney-Drazin Theorems for Waves oin Axismmetric Mean Flows in Compressible Atmospheres. *Journal of Atmospheric Sciences*, *35*, 175. Retrieved from http://journals.ametsoc.org/doi/abs/10.1175/1520-0469(1978)035%3C0175:GEPACD%3E2.0.CO;2 doi: 10.1175/1520-0469(1978)035⟨0175:gepacd⟩2.0.co;2

Arblaster, J. M., & Meehl, G. A. (2006, 6). Contributions of External Forcings to Southern Annular Mode Trends. *Journal of Climate*, *19*(12), 2896–2905. Retrieved from http://journals.ametsoc.org/doi/abs/10.1175/JCLI3774.1 doi: 10.1175/JCLI3774.1

Arblaster, J. M., Meehl, G. A., & Karoly, D. J. (2011). Future climate change in the Southern Hemisphere: Competing effects of ozone and greenhouse gases. *Geophysical Research Letters*, *38*(2), 1–6. doi: 10.1029/2010GL045384

Baldwin, M. P., & Dunkerton, T. J. (1999, 12). Propagation of the Arctic Oscillation from the stratosphere to the troposphere. *Journal of Geophysical Research Atmospheres*, *104*(D24), 30937–30946. doi: 10.1029/1999JD900445

Baldwin, M. P., & Dunkerton, T. J. (2001, 10). Stratospheric harbingers of anomalous weather regimes. *Science (New York, N.Y.)*, *294*(5542), 581–4. Retrieved from http://www.ncbi.nlm.nih.gov/pubmed/11641495 doi: 10.1126/science.1063315

Charlton, A. J., & Polvani, L. M. (2007, 2). A New Look at Stratospheric Sudden Warmings. Part I: Climatology and Modeling Benchmarks. *Journal of Climate*, *20*(3), 449–469. Retrieved from http://journals.ametsoc.org/doi/abs/10.1175/JCLI3996.1 doi: 10.1175/JCLI3996.1

Chen, P., & Robinson, W. A. (1992, 12). Propagation of planetary waves between the troposphere and stratosphere. *Journal of Atmospheric Sciences*, *49*(24), 2533. Retrieved from http://adsabs.harvard.edu/abs/1992JAtS...49.2533Chttp://journals.ametsoc.org/doi/abs/10.1175/1520-0469(1992)049%3C2533:POPWBT%3E2.0.CO;2 doi: 10.1175/1520-0469(1992)049⟨2533:POPWBT⟩2.0.CO;2

Domeisen, D. I., Butler, A. H., Charlton-Perez, A. J., Ayarzagüena, B., Baldwin, M. P., Dunn-Sigouin, E., ... Taguchi, M. (2020). The Role of the Stratosphere in Subseasonal to Seasonal Prediction: 2. Predictability Arising From Stratosphere-Troposphere Coupling. *Journal of Geophysical Research: Atmospheres*, *125*(2), 1–20. doi: 10.1029/2019JD030923

Eliassen, A., & Palm, T. (1960). On the transfer of energy in stationary mountain waves. *Geofys. Publ.*, *22*(3), 1–23.

Gerber, E. P., Baldwin, M. P., Akiyoshi, H., Austin, J., Bekki, S., Braesicke, P., ... Smale, D. (2010). Stratosphere-troposphere coupling and annular mode variability in chemistry-climate models. *Journal of Geophysical Research Atmospheres*, *115*(18), 1–15. doi: 10.1029/2009JD013770

Gerber, E. P., & Vallis, G. K. (2009, 2). On the Zonal Structure of the North Atlantic Oscillation and Annular Modes. *Journal of the Atmospheric Sciences*, *66*(2), 332–352. Retrieved from http://journals.ametsoc.org/doi/abs/10.1175/2008JAS2682.1https://journals.ametsoc.org/jas/article/66/2/332/26691/On-the-Zonal-Structure-of-the-North-Atlantichttps://journals.ametsoc.org/doi/10.1175/2008JAS2682.1 doi: 10.1175/

2008JAS2682.1

Gillett, N. P., Kell, T. D., & Jones, P. D. (2006). Regional climate impacts of the Southern Annular Mode. *Geophysical Research Letters*, *33*(23), 1–4. doi: 10.1029/2006GL027721

Grise, K. M., Polvani, L. M., Tselioudis, G., Wu, Y., & Zelinka, M. D. (2013, 7). The ozone hole indirect effect: Cloud-radiative anomalies accompanying the poleward shift of the eddy-driven jet in the Southern Hemisphere. *Geophysical Research Letters*, *40*(14), 3688–3692. Retrieved from http://doi.wiley.com/10.1002/grl.50675 doi: 10.1002/grl.50675

Grise, K. M., Thompson, D. W. J., & Forster, P. M. (2009, 8). On the Role of Radiative Processes in Stratosphere–Troposphere Coupling. *Journal of Climate*, *22*(15), 4154–4161. Retrieved from http://journals.ametsoc.org/doi/abs/10.1175/2009JCLI2756.1 doi: 10.1175/2009JCLI2756.1

Haynes, P. H., McIntyre, M. E., Shepherd, T. G., Marks, C. J., & Shine, K. P. (1991, 2). On the "Downward Control" of Extratropical Diabatic Circulations by Eddy-Induced Mean Zonal Forces. *Journal of the Atmospheric Sciences*, *48*(4), 651–678. Retrieved from http://journals.ametsoc.org/doi/abs/10.1175/1520-0469(1991)048%3C0651:OTCOED%3E2.0.CO;2 doi: 10.1175/1520-0469(1991)048⟨0651:OTCOED⟩2.0.CO;2

Hendon, H. H., Lim, E. P., & Abhik, S. (2020). Impact of Interannual Ozone Variations on the Downward Coupling of the 2002 Southern Hemisphere Stratospheric Warming. *Journal of Geophysical Research: Atmospheres*, *125*(16), 1–16. doi: 10.1029/2020JD032952

Hersbach, H., Bell, B., Berrisford, P., Hirahara, S., Horányi, A., Muñoz-Sabater, J., ... Thépaut, J. (2020, 7). The ERA5 global reanalysis. *Quarterly Journal of the Royal Meteorological Society*, *146*(730), 1999–2049. Retrieved from https://onlinelibrary.wiley.com/doi/abs/10.1002/qj.3803 doi: 10.1002/qj.3803

Hurrel, J. W., & Van Loon, H. (1994, 5). A modulation of the atmospheric annual cycle in the Southern Hemisphere. *Tellus A*, *46*(3), 325–338. Retrieved from http://tellusa.net/index.php/tellusa/article/view/15482 doi: 10.1034/j.1600-0870.1994.t01-1-00007.x

Jucker, M. (2016, 12). Are Sudden Stratospheric Warmings Generic? Insights from an Idealized GCM. *Journal of the Atmospheric Sciences*, *73*(12), 5061–5080. Retrieved from http://journals.ametsoc.org/doi/10.1175/JAS-D-15-0353.1 doi: 10.1175/JAS-D-15-0353.1

Jucker, M. (2021a). *aostools.* Zenodo. Retrieved from https://github.com/mjucker/aostools doi: 10.5281/zenodo.597598

Jucker, M. (2021b, 4). Scaling of Eliassen-Palm flux vectors. *Atmospheric Science Letters*, *22*(4), e1020. Retrieved from https://onlinelibrary.wiley.com/doi/10.1002/asl.1020 doi: 10.1002/asl.1020

Jucker, M., & Gerber, E. P. (2017, 9). Untangling the Annual Cycle of the Tropical Tropopause Layer with an Idealized Moist Model. *Journal of Climate*, *30*(18), 7339–7358. Retrieved from http://journals.ametsoc.org/doi/10.1175/JCLI-D-17-0127.1 doi: 10.1175/JCLI-D-17-0127.1

Lim, E.-P., Hendon, H. H., Boschat, G., Hudson, D., Thompson, D. W. J., Dowdy, A. J., & Arblaster, J. M. (2019, 11). Australian hot and dry extremes induced by weakenings of the stratospheric polar vortex. *Nature Geoscience*, *12*(11), 896–901. Retrieved from http://dx.doi.org/10.1038/s41561-019-0456-xhttp://www.nature.com/articles/s41561-019-0456-x doi: 10.1038/s41561-019-0456-x

Lim, E.-P., Hendon, H. H., Butler, A. H., Thompson, D. W. J., Lawrence, Z., Scaife, A. A., ... Wang, G. (2021, 2). The 2019 Southern Hemisphere stratospheric polar vortex weakening and its impacts. *Bulletin of the American Meteorological Society*, 1–50. Retrieved from https://journals.ametsoc.org/

view/journals/bams/aop/BAMS-D-20-0112.1/BAMS-D-20-0112.1.xml doi: 10.1175/BAMS-D-20-0112.1

Marshall, G. J. (2003, 12). Trends in the Southern Annular Mode from Observations and Reanalyses. *Journal of Climate*, *16*(24), 4134–4143. Retrieved from http://journals.ametsoc.org/doi/abs/10.1175/1520-0442%282003%29016%3C4134%3ATITSAM%3E2.0.CO%3B2 doi: 10.1175/1520-0442(2003)016⟨4134:TITSAM⟩2.0.CO;2

McLandress, C., Shepherd, T. G., Scinocca, J. F., Plummer, D. A., Sigmond, M., Jonsson, A. I., & Reader, M. C. (2011). Separating the dynamical effects of climate change and ozone depletion. Part II: Southern Hemisphere troposphere. *Journal of Climate*, *24*(6), 1850–1868. doi: 10.1175/2010JCLI3958.1

Neale, R. B., Richter, J. H., Conley, A. J., Park, S., Lauritzen, P. H., Gettelman, A., & Williamson, D. L. (2010). Description of the NCAR Community Atmosphere Model (CAM 4.0). *NCAR Technical Note*, *TN-485*(April), 1–196.

Oleson, K. W., Lawrence, D. M., Bonan, G. B., Flanner, M. G., Kluzek, E., Lawrence, P. J., ... Thornton, P. E. (2010). Technical Description of version 4.0 of the Community Land Model (CLM). *NCAR Technical Note*, *TN-478*(April), 1–238. doi: http://dx.doi.org/10.5065/D6FB50WZ

Plumb, R. A. (2002). Stratospheric Transport. *J. Meteor. Soc. Japan*, *80*(1949), 793–809.

Plumb, R. A., & Semeniuk, K. (2003). Downward migration of extratropical zonal wind anomalies. *Journal of Geophysical Research*, *108*(D7), 4223. Retrieved from http://doi.wiley.com/10.1029/2002JD002773 doi: 10.1029/2002JD002773

Rae, C. D., Keeble, J., Hitchcock, P., & Pyle, J. A. (2019). Prescribing Zonally Asymmetric Ozone Climatologies in Climate Models: Performance Compared to a Chemistry-Climate Model. *Journal of Advances in Modeling Earth Systems*, *11*(4), 918–933. doi: 10.1029/2018MS001478

Randel, W. J., & Cobb, J. B. (1994). Coherent variations of monthly mean total ozone and lower stratospheric temperature. *Journal of Geophysical Research*, *99*(D3), 5433. Retrieved from http://doi.wiley.com/10.1029/93JD03454 doi: 10.1029/93JD03454

Rao, J., Garfinkel, C. I., White, I. P., & Schwartz, C. (2020, 7). The Southern Hemisphere Minor Sudden Stratospheric Warming in September 2019 and its Predictions in S2S Models. *Journal of Geophysical Research: Atmospheres*, *125*(14). Retrieved from https://onlinelibrary.wiley.com/doi/10.1029/2020JD032723 doi: 10.1029/2020JD032723

Safieddine, S., Bouillon, M., Paracho, A. C., Jumelet, J., Tencé, F., Pazmino, A., ... Clerbaux, C. (2020). Antarctic Ozone Enhancement During the 2019 Sudden Stratospheric Warming Event. *Geophysical Research Letters*, *47*(14), 1–10. doi: 10.1029/2020GL087810

Sigmond, M., Scinocca, J. F., Kharin, V. V., & Shepherd, T. G. (2013, 1). Enhanced seasonal forecast skill following stratospheric sudden warmings. *Nature Geoscience*, *6*(2), 98–102. Retrieved from http://www.nature.com/doifinder/10.1038/ngeo1698 doi: 10.1038/ngeo1698

Simpson, I. R., Blackburn, M., & Haigh, J. D. (2009, 5). The Role of Eddies in Driving the Tropospheric Response to Stratospheric Heating Perturbations. *Journal of the Atmospheric Sciences*, *66*(5), 1347–1365. Retrieved from http://journals.ametsoc.org/doi/abs/10.1175/2008JAS2758.1 doi: 10.1175/2008JAS2758.1

Thompson, D. W., & Wallace, J. M. (1998, 5). The Arctic oscillation signature in the wintertime geopotential height and temperature fields. *Geophysical Research Letters*, *25*(9), 1297–1300. doi: 10.1029/98GL00950

Thompson, D. W. J., Baldwin, M. P., & Solomon, S. (2005, 3). Stratosphere–Troposphere Coupling in the Southern Hemisphere. *Journal of the*

Atmospheric Sciences, *62*(3), 708–715. Retrieved from http://journals.ametsoc.org/doi/abs/10.1175/JAS-3321.1 doi: 10.1175/JAS-3321.1

Thompson, D. W. J., Solomon, S., Kushner, P. J., England, M. H., Grise, K. M., & Karoly, D. J. (2011, 10). Signatures of the Antarctic ozone hole in Southern Hemisphere surface climate change. *Nature Geoscience*, *4*(11), 741–749. Retrieved from http://www.nature.com/doifinder/10.1038/ngeo1296 doi: 10.1038/ngeo1296

Ummenhofer, C. C., England, M. H., McIntosh, P. C., Meyers, G. A., Pook, M. J., Risbey, J. S., ... Taschetto, A. S. (2009, 2). What causes southeast Australia's worst droughts? *Geophysical Research Letters*, *36*(4), L04706. Retrieved from http://doi.wiley.com/10.1029/2008GL036801 doi: 10.1029/2008GL036801

Vitart, F., Ardilouze, C., Bonet, A., Brookshaw, A., Chen, M., Codorean, C., ... Zhang, L. (2017). The subseasonal to seasonal (S2S) prediction project database. *Bulletin of the American Meteorological Society*, *98*(1), 163–173. doi: 10.1175/BAMS-D-16-0017.1

Methods

Stratospheric Warming Events (SWE)

For the purposes of this study, we define an SWE very loosely as a dynamically driven event where the stratospheric polar cap geopotential height and stratospheric ozone concentration become anomalously high within a few weeks in Austral spring. It is not the purpose of this work to apply any specific definition, such as a sudden stratospheric warming (SSW). Rather, we study the 2019 spring evolution and make more general statements based on our idealised model simulations (see below).

Reanalysis data

We use data from ERA5 reanalysis (Hersbach et al., 2020) both as representation of the atmosphere in spring 2019 and to force our model simulations. The climatologies are constructed with data from 2005-2015, which is long enough for our purposes, and avoids the ozone hole formation, long-term greenhouse induced climate change, the 2002 and 2019 sudden stratospheric warmings as well as the 2016 Antarctic sea ice decline.

Ozone perturbations

Ozone perturbation files were created for forcing the models described below. All data was downloaded from ERA5 as described above. In order to only include perturbations related to the 2019 SWE, we use climatological ozone corresponding to the years 2005-2015 from day of year 150 (June 1) to 230 (August 18) and 2019/2020 ozone from day 250 (September 7) to 130 (May 10), with a linear transition from 2019/2020 to climatology between May 10 and June 1 and from climatology to 2019/2020 between August 18 and September 7. As an example, Fig. 5 shows polar cap averaged total column ozone for climatology and perturbation runs. These values are then averaged by calendar month to be used as model input (dashed lines).

Community Atmosphere Model (CAM4)

We use the National Center for Atmospheric Research (NCAR) Community Atmosphere Model Version 4 (CAM4 (Neale et al., 2010)) which is coupled to the Community Land Model Version 4 (CLM4 (Oleson et al., 2010)). CAM4 is run with a 1.875×2.5 degree finite volume grid with 26 hybrid sigma levels. CAM4 is forced with monthly climatological SSTs and sea-ice relative to 1850. Two simulations are carried out in a pre-industrial control setup with only difference being the ozone fields used in the simulations. The control and perturbation simulations use different ozone concentrations as described above. Both simulations are run for 50 years and the last 30 years are used for the analysis presented in this study.

Seasonal forecasting data

We use data from the ECMWF S2S database (Vitart et al., 2017) from the models labeled in Fig. 1 with forecast initialization between August 16 and 31 2019. Since the authors didn't have model climatologies available to compute anomaly fields, Fig. 1(b) shows the cosine latitude weighted average of 30-60°S minus 60-90°S 500 hPa geopotential height, which is then compared to the same data from ERA5 (Hersbach et al., 2020).

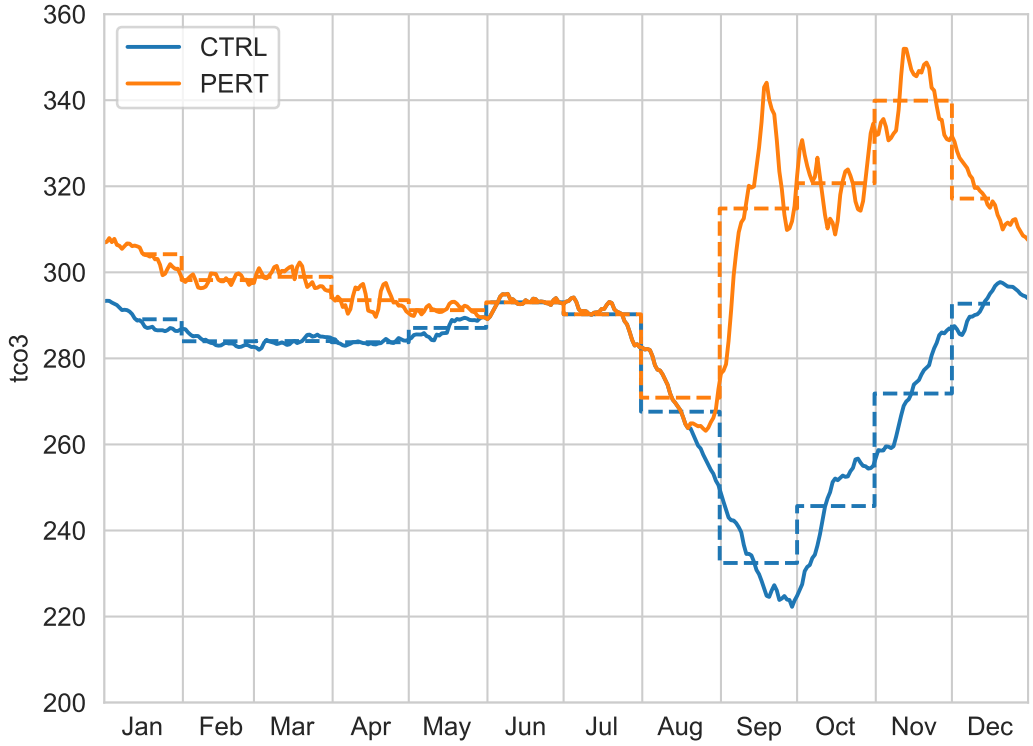

Figure 5. Climatological and perturbation polar cap (60-90°S) mean total column ozone. Dashed lines show monthly means as used in the model simulations.

Model of an idealized Moist Atmosphere (MiMA)

MiMA (Jucker & Gerber, 2017) was run in a configuration similar to when it was first introduced, but with surface temperature fixed to ERA5 September skin temperature climatology (as described above), and solar forcing was fixed to the equivalent of mid-September. The model solves the fully nonlinear primitive equations on the sphere and includes full radiative transfer calculations including fixed 3D ozone and interactive water vapor, but there are no clouds and a relatively simple convection scheme. As surface temperature is fixed there is no interaction with the surface mixed layer ocean other than evaporation and surface drag. All simulations shown here were run with a T42 (approx. 2.5 degree) resolution and 40 vertical levels extending up to 0.15 hPa and realistic orography. Atmospheric initial conditions were taken from ERA5 September climatology, and an initial spinup of 1000 days was performed. Starting from common spinup, two 30-member ensembles were run, where each ensemble was created by randomly perturbing the initial temperature field by a maximum of 0.1 K throughout the atmosphere. The control ensemble used climatological September mean ozone and the perturbation ensemble used September mean ozone from the year 2019 as described above.

Southern Annular Mode

The Southern Annular Mode (SAM) has multiple definitions which are equivalent for most purposes. One of the most widely used definitions by both oceanographers and atmospheric scientists is the 'Marshall Index' (Marshall, 2003) which is based on station data and defines the SAM as the means sea level pressure difference between

six stations located around 37-47°S and six stations located around 65-71°S. However, SAM's attractiveness is that it identifies the main mode of variability of the hemisphere, and therefore another widely used definition is the first empirical orthogonal function (EOF) of certain large scale atmospheric variables (usually zonal wind or geopotential height). One advantage of this method is that the EOF can be calculated at every pressure level throughout the atmosphere, resulting in a SAM value at each pressure level and point in time (D. W. Thompson & Wallace, 1998; Baldwin & Dunkerton, 1999; Gerber et al., 2010). Throughout the atmosphere, the first EOF of geopotential height is a dipole between low and high latitudes (Gerber et al., 2010) (Fig. S3), such that it can be approximated by simply calculating the polar cap geopotential height anomaly at each pressure level. This has the advantage that we don't need a long timeseries of data to compute the first EOF (nor to standardize with variance), which is important for our seasonal forecasting as well as the short ensemble simulations with MiMA.

Eliassen-Palm fluxes

Eliassen-Palm (EP) flux is an important tool to diagnose wave-mean flow interaction, as its direction indicates the propagation of wave activity flux and its divergence is directly related to the residual overturning circulation (Eliassen & Palm, 1960; Andrews & McIntyre, 1978). In pressure coordinates, the components are (Andrews et al., 1983):

$$f_\phi = -\overline{u'v'}, \tag{1}$$

$$f_p = \left(f - \frac{1}{a\cos\phi}\frac{\partial(\bar{u}\cos\phi)}{\partial\phi}\right)\frac{\overline{v'\theta'}}{\bar{\theta}_p}, \tag{2}$$

and

$$\mathbf{F} \equiv (F_\phi, F_p) = a\cos\phi(f_\phi, f_p). \tag{3}$$

Here, u, v are the zonal and meridional wind, θ potential temperature, a Earth's radius and ϕ latitude. Overline ($\bar{\cdot}$) denotes zonal mean and prime ($'$) deviation from zonal mean. We used the recently derived scaling of Jucker (2021b), which was calculated and plotted using `aostools` (Jucker, 2021a).

Downward control

Downward control refers to the findings from wave-mean flow interaction theory that the residual mean meridional overturning circulation is proportional to the vertical integral of wave activity flux above any given level (Andrews et al., 1987; Haynes et al., 1991):

$$\overline{\psi}^*(\phi, z) = \int_z^\infty \left.\frac{\rho_0 a \nabla\cdot\mathbf{F}\cos^2\phi}{\overline{m}_\phi}\right|_{\phi=\phi(z')}, \tag{4}$$

where ψ^* is the residual streamfunction in the latitude-height plane, ρ_0 is the density of air, a Earth's radius, ϕ latitude, z height and m_ϕ the angular momentum per unit mass. $\nabla\cdot\mathbf{F}$ is Eliassen-Palm flux divergence and represents the zonal force per unit mass (Andrews & McIntyre, 1976). Overline ($\bar{\cdot}$) denotes zonal mean. The integral is taken along constant angular momentum $\overline{m}_\phi$, but in practice is done along constant latitude as contours of angular momentum are at nearly constant latitude (Haynes et al., 1991).

Supporting Information for "Ozone-forced Southern Annular Mode during Antarctic Stratospheric Warming Events"

M. Jucker[1], R. Goyal[1]

[1]Climate Change Research Centre, University of New South Wales, Sydney, Australia

Contents of this file

1. Text S1 to S2
2. Figures S1 to S2
3. Table S1

Text S1 - Correlation between IOD and SAM: To determine the correlation between the Indian Ocean Dipole and the Southern Annular Mode, we compare the monthly Marshall SAM index (`http://www.nerc-bas.ac.uk/public/icd/gjma/newsam.1957.2007.txt`, downloaded 2021-06-17) and the Dipole Mode Index (`https://psl.noaa.gov/gcos_wgsp/Timeseries/Data/dmi.had.long.data`, downloaded 2021-06-17) on monthly, seasonal, and yearly timescales, with the results shown in Table S1.

Text S2 - Stratospheric ozone vs. SAM in ERA5: Besides the years 2002 and 2019 which are known for their SWEs, two earlier years are also marked with extremely high

polar cap total column ozone values (marked red in Fig. S1, left). All four years show the vertical dipole of polar cap geopotential height anomalies seen in 2019, albeit in a less prominent way. While it is only as obvious in 1979, it is still visible during the first and last ozone peaks in 1988 (beginning September and November) and during the very short large ozone peak in 2002 (last few days of September and first few days of October).

monthly	DJF	MAM	JJA	SON	yearly
0.104	0.358	0.209	0.204	-0.096	0.247

Table S1. Correlation coefficients between IOD and SAM.

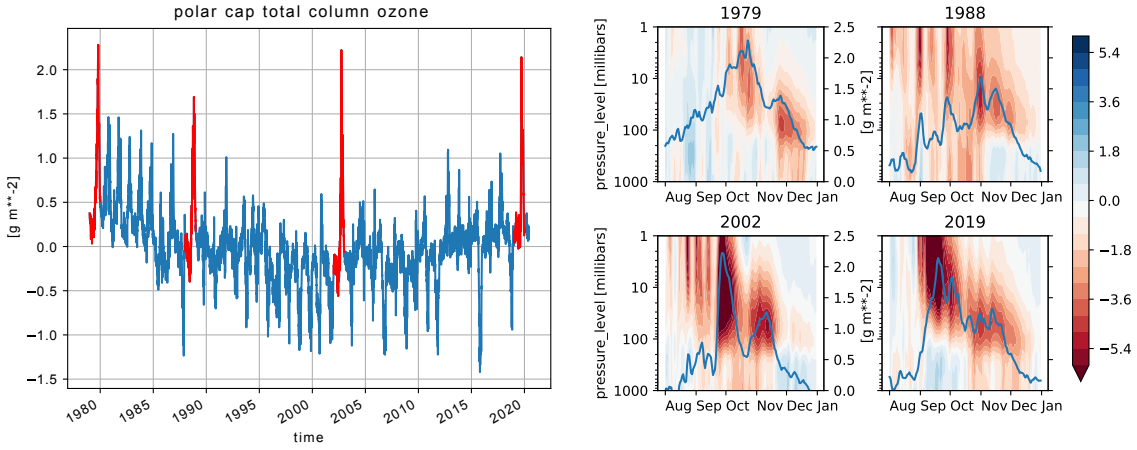

Figure S1. ERA5 polar cap total column ozone and geopotential height anomalies. (left) Total column ozone timeseries for the complete record (minus 1979-2020 seasonal climatology). (right) Same as Fig. 1a) but for the four years of large peaks in the ozone timeseries (marked red on left).

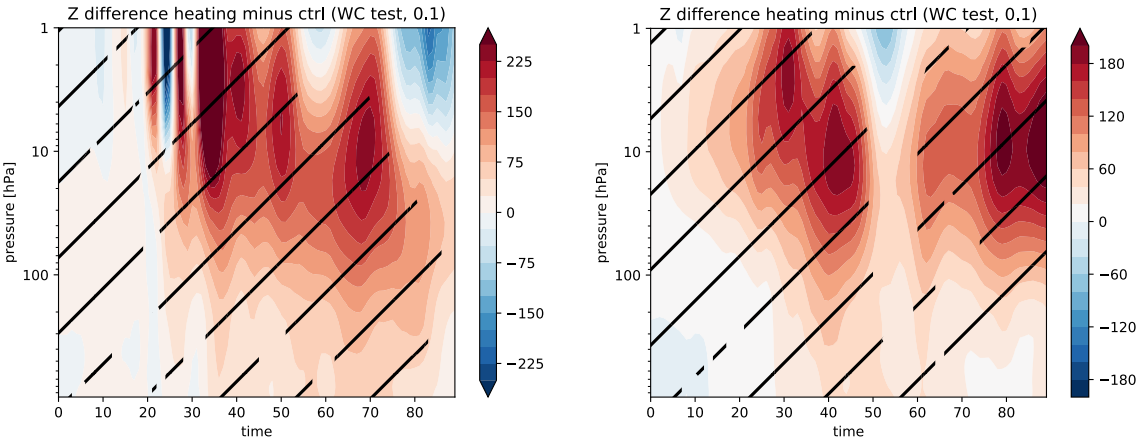

(a) Same as Fig. 2(b) but starting in August.

(b) Same as Fig. 2(b) but starting in October.

Figure S2. Polar cap geopotential height anomalies for simulations with MiMA where solar forcing corresponds to 30 days earlier (i.e. August, left) or later (October, right).

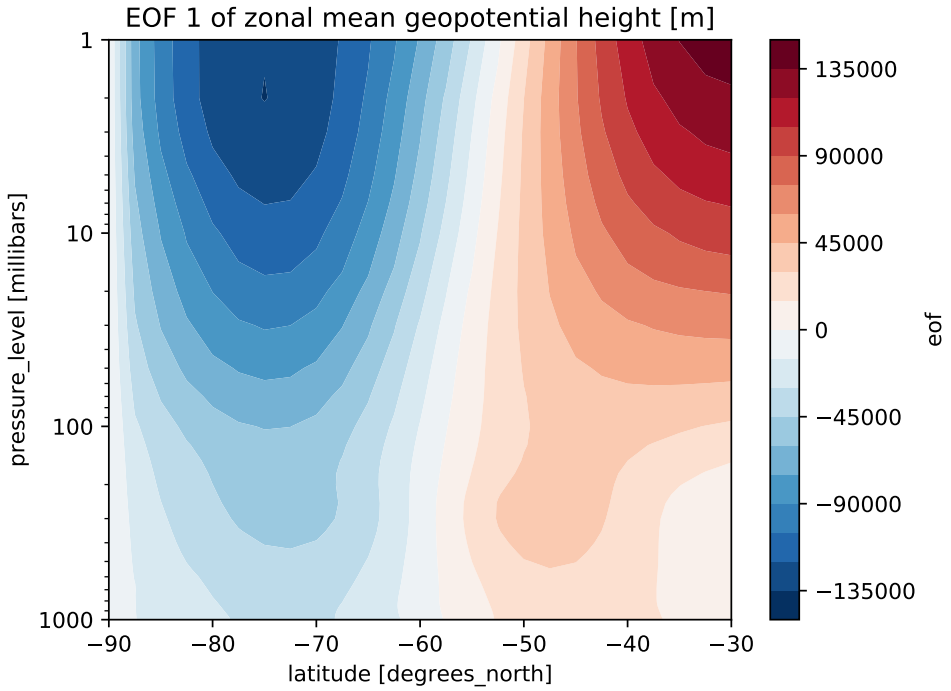

Figure S3. First Empirical Orthogonal Function (EOF) of de-seasonalised zonal mean geopotential anomalies from ERA5 data (1979-2019)). The standardised timeseries of the first principle component at each pressure level is identified as the Southern Annular Mode index.